ISSN: 2230-9926

Available online at http://www.journalijdr.com

IJDR

International Journal of Development Research
Vol. 10, Issue, 10, pp. 41498-41502, October, 2020
https://doi.org/10.37118/ijdr.20311.10.2020

RESEARCH ARTICLE OPEN ACCESS

STRUCTURAL AND ELECTRICAL PROPERTIES OF THECERAMICS BASED ON SPINEL $Mn_xCo_{1-x}Al_2O_4$ COMPOUNDS

Keydson Quaresma Gomes[1*], K. M. M.Eiras[1] and A. B. S. Lavinscky[2]

[1]Department of Engineering and Technology, Federal University of Espírito Santo, Brazil
[2]Nanomaterials and Advanced Ceramics Laboratory, Institute of Physics, University of São Paulo, Brazil

ARTICLE INFO

Article History:
Received 14th July, 2020
Received in revised form
09th August, 2020
Accepted 07th September, 2020
Published online 30th October, 2020

Key Words:
Impedance spectroscopy,
Structural properties, Electrical properties,
X-ray diffraction, Spinel.

Corresponding author:
Keydson Quaresma Gomes

ABSTRACT

Ceramic pellets of $Mn_xCo_{1-x}Al_2O_4$ compounds were investigated by powder X-ray diffraction method, as well as electrical properties with resistance analysis by the two-point method and complex impedance measurements. The manganese oxide was added to the system at molar fraction ratios of x = 0.05, 0.30, 0.50, 0.70, and 0.95. It was obtained samples from these compositions and were sintered at 1773 K for 5 h. The X-ray diffraction results were refined by the Rietveld method, and thus, we could determine the type of structure system as being spinel. The results of the AC electrical response (impedance spectroscopy) showed that at lower frequencies the largest contribution to the conductivity of the sample comes from the grain boundary. The best conductivity was observed in the $Mn_{0.50}Co_{0.50}Al_2O_4$ sample.

Citation: ***Keydson Quaresma Gomes, K. M. M.Eiras and A. B. S. Lavinscky, 2020.*** "Structural and electrical properties of theceramics based on spinel MnxCo1-xAl2O4 compounds*", International Journal of Development Research*, 10, (10), 41498-41502.

INTRODUCTION

Over the years, some transition metals (Cu, Mn, Fe, Co, Zn, etc.) have been used for gas, temperature, and humidity sensing applications. The low-cost relative of oxide materials based on transition metals makes them be the subject of several studies.(Hotovy *et al*., 1999; Oh *et al*., 2009; Youl Bae and Man Choi, 1999) The presence of structural defects and the degree of non-stoichiometry are interesting features for materials with this functionality. The spinel compounds have a structure with a tetrahedral arrangement with a high density of defects and semiconductor nature. The spinel structure belongs to Fd3m group with structural formula MX_2O_4. Besides, the unitary cell of this structure contains 32 oxygen atoms compressed in a cubic structure with 8 equivalent positions for tetrahedral coordination M^{2+} cations, A-sites, and 16 equivalent positions for octahedral coordination X^{3+} cations, B-sites.(Porta *et al*., 1979; Sickafus *et al*., 2004) In particular, cobalt ($CoAl_2O_4$) and copper ($CuAl_2O_4$) aluminates spinel became attractive in recent years due to its structural, thermal, chemical, optical, and electrical properties for many applications.

These aluminates have been used as catalysts, color filters for automotive lamps or pigment layer on luminescent materials, gas sensor, photocatalytic water splitting, solar absorber, among others.(Abaide *et al*., 2015; El Habra *et al*., 2007; Gomes, 2003; Zasada *et al*., 2014) Procedures as combustion, Pechini, sol-gel, and reverse microemulsion are some of the most used processes for obtaining these compounds.(Abaide *et al*., 2015) One of the main reasons for studying these materials based on $CoAl_2O_4$(El Habra *et al*., 2007; Zasada *et al*., 2014) is the fact they exhibit similar characteristics to the $CuAl_2O_4$(Gomes, 2003), but with a more resistive electrical response.This paper aimed to investigate ceramic samples of $CoAl_2O_4$ oxide adding Mn^{2+} ions, forming the MnO-CoO-Al_2O_3 spinel system, to gain a better understanding of their structural and electrical properties by the effect of manganese.

Experimental Procedure: For experimental, the following raw materials were applied: Alumina powder, Al_2O_3 (Alcoa A-16; 99.8% purity), Cobalt Sulphate, $CoSO_4.7H_2O$ (LabSynth; 99.0% purity), and Manganese Sulfate, $MnSO_4.H_2O$ (Mallinckrodt; 99.68% purity). Samples were prepared according to stoichiometric compositions of $Mn_xCo_{1-x}Al_2O_4$ chemical structure with x as 0.05, 0.30, 0.50, 0.70, and 0.95

molar fractions.Powders were obtained following the precipitation method used by Gallagher *et al*. (Gallaghe *et al*., 1969) Cobalt sulfate, manganese sulfate, aluminum oxide, and ammonium oxalate solutions were prepared using deionized water as a diluent as 1:1 proportion in the stoichiometric calculation. To ensure the precipitation, solutions were kept under constant stirring over a 363 K hotplate for approximately 30 min. The precipitated material was filtered, exhaustively washed in Milli-Q water to eliminate sulfate ions traces, and dried at 383 K per 24 h. The material was de-agglomerated in a mortar and sifted through a 60 mesh sieve and then calcined at 873 K per 2 h. After pre-treatment, the material was again de-agglomerated for 1 h in a planetary ball mill, then dried at 383 K per 24 h and again sifted through a 60 mesh sieve. Powdered materials were mixed with a small amount of PVAL (polyvinyl alcohol) 10% binder to obtain monolithic pellets (diameter 20 mm and thickness 3 mm) in a press which load was 2 tons. The pellets were sintered at 1773 K per 5 h in a furnace at a constant heating rate of 278 K/min.Powdered samples obtained by de-agglomeration of sintered pellets in an ABNT 325 mesh were used to verify the spinel phase formation by powder X-ray diffraction (XRD) analysis. Powder XRD patterns were recorded on a SiemensD5005 diffractometer using Cu-K_α radiation (λ = 1.5418 Å). The scanning was performed in a step-by-step sequence with an increment of 0.033° (2θ), for a count time of 3s. The XRD data collected were used as data to the structural refinements through DBWS 98 software(Bleicher *et al*., 2000; Young *et al*., 1995) employing the Rietveld method(Rietveld, 1969).Pellet samples were treated with silver paste on the adjacent faces, resulting in the formation of a parallel plate capacitor. DC electrical measurements were realized applying the two-point method (one probe on each of the two resistor leads). It was usedthe HP3457A and HP3458A multimeters in a chamber at 723 K maxim temperature, and a microcomputer equipped with an HP-IB interface card and HP VEE 3.0 software(Microsoft, 2000). The AC measurements were carried out by HP4192A impedance meter coupled to a temperature chamber in a frequency range of 5Hz - 13MHz and the data were analyzed using Data Analysis software(Schwake *et al*., 1998). Impedance diagrams were fitted by equivalent circuits simulation using calculations of the real and imaginary impedance parts.

RESULTS AND DISCUSSION

Structural Characterization: Figure 1 presents the X-ray diffraction (XRD) patterns of sintered samples at 1773 K by 5 hours in the $Mn_xCo_{1-x}Al_2O_4$ system for x = 0.05; 0.30; 0.50; 0.70; 0.95. The XRD analysis indicated the presence of phases alumina (Al_2O_3) and centered cubic spinel structure solid solution ($Mn_xCo_{1-x}Al_2O_4$). These phases were also observed for the samples heat-treated at 1273 and 1573 K (not shown) in all compositions of the system. Possibly a concurrent diffusion between Co^{2+} and Al^{3+} ions occurred, where an Al^{3+} ions content rapidly diffused toward the surface in the initial stage of the reaction forming the Al_2O_3 phase, and the remaining quantity led to the formation of the $Mn_xCo_{1-x}Al_2O_4$ compounds.(Bolt *et al*., 1998) This suggests it requires higher temperatures to complete structural changes and forming a single phase. Pradhan *et al*.(Pradhan *et al*., 2019) investigated the optical magnetic properties of $Co_{1-x}Mn_xAl_2O_4$ compounds with 0 < x < 0.30 prepared by solid state reaction and heat-treated at 1403-1423 K for 24h.

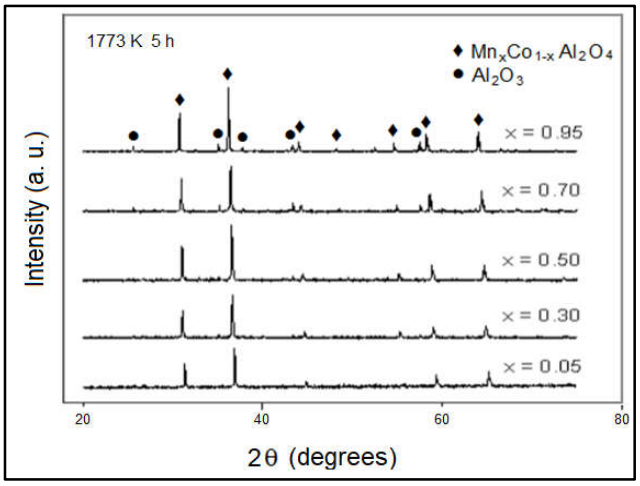

Figure 1. XRD patterns of the $Mn_xCo_{1-x}Al_2O_4$ samples sintered at 1773 K

They reported the presence of the MnO phase for x above 0.30 and not found any secondary phases for 0 < x < 0.30. It was noted a narrowing of diffraction peaks as the temperature increases, it associated with an increase in the crystallite size.A slight shift in peak positions to smaller angles can be seen in Figure 1 as a direct consequence of Co^{2+} ions are being replaced by the Mn^{2+} ions in the $CoAl_2O_4$ lattice. This behavior is due to the small difference between their ionic radii, the Mn^{2+} ion ($r_{ion}^{Mn^{2+}} = 0.66$ Å) is greater than Co^{2+} ion ($r_{ion}^{Co^{2+}} = 0.58$ Å) according to their coordination numbers (Shannon, 1976). An increase in the lattice parameter as increasing of manganese amount was observed by the results of Rietveld refinement corroborating with those of XRD patterns. These results are similar to those observed in other studies (Pradhan *et al*., 2019). XRD patterns were used as input data in the Rietveld method to quantify the present phases in the compositions and good results were obtained in all cases. The Rietveld refinement was performed to the sintered samples at 1773, 1573, and 1273 K, and in all temperatures, it was identified the alumina and $Mn_xCo_{1-x}Al_2O_4$ spinel phases. The spinel phase had the biggest proportion in mass fraction correspondent to 86% of the mass fraction total of the sample and the others 14% were identified as alumina. This indicates the chemical reaction between the precursors(MnO, CoO, and Al_2O_3) was not totally converted into $Mn_xCo_{1-x}Al_2O_4$ solid solution.

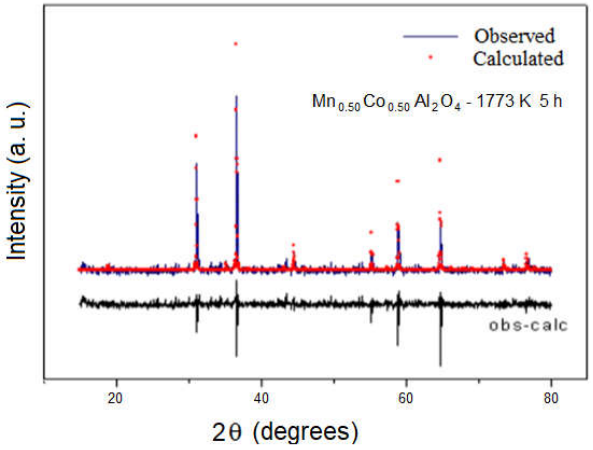

Figure 2. Structural refinement by the Rietveld method of $Mn_{0.5}Co_{0.5}Al_2O_4$ compound sintered at 1773 K. Observed (blue line); calculated (red line); obs-calc (black line) difference between observed and calculated data.

According to the fitting of crystallographic parameters, the solid solution phase was confirmed as belonging to the space group *Fd3m*. Figure 2 illustrates an example of the refinement of the $Mn_{0.50}Co_{0.50}Al_2O_4$ sample by the Rietveld method.Figure 3 presents the composition-dependent evolution of the lattice parameter of the $Mn_xCo_{1-x}Al_2O_4$ system. Lattice constant values are increased as the Co^{2+} is being replaced by Mn^{2+}, because the ionic radii of cobalt is lower than manganese one. The octahedra formed by Co^{2+} ions give rise to new ones formed by Mn^{2+} causing the enlargement of the primitive cell volume. This behavior follows a linear pattern consistent with Vegard's law(Jacob *et al*., 2007; Lambregts and Frank, 2004), indicating that Mn^{2+} ions are systematically substituted at the Co^{2+} sites of the $CoAl_2O_4$ compound at a constant temperature. Similarly, Pradhan *etal*.(Pradhan *et al*., 2019) also observed the same phenomenon.Previously studies noticed that many spinel symmetry compounds can accommodate significant amounts of cation disorder, at so-called "variate atom equipoints".(Barth and Posnjak, 2014, 1931; Posnjak and Barth, 1931) In the literature, the A-sites for tetrahedral sites and B-sites for octahedral sites convention is often used.(Sickafus *et al*., 2004)Besides, these cations have limited configurations called "normal spinel" and "inverse spinel".(Verwey and Heilmann, 1947). The Rietveld method also made it possible to estimate the concentration of divalent ions in octahedral sites by the occupancy factor parameter. The results indicated that there is a strong preference for the Co^{2+} and Mn^{2+} ions to occupy A-sites(Sickafus *et al*., 2004). However, considering the octahedrally coordinated Co^{2+} and the structure inversion parameters(Sickafus *et al*., 2004), the analysis indicated that the structure is a partially inverse spinel because it has a considerable volume of Co^{2+} ions in B-sites. On the other hand, the structure for Mn^{2+} ions was close to normal spinel, due to the small volume of these ions octahedrally coordinated. These results are similar to those obtained by Jacob and Fitzner(Jacob and Fitzner, 1977), where they observed a redistribution of Co^{2+} ions in B-sites. They reported the reason for the higher concentration of Co^{2+} in B-sites is directly associated with the Mn^{2+} ion insertion in the $Mn_xCo_{1-x}Al_2O_4$ system and its preferential occupancy. The manganese divalent ion has a stabilization energy in A-sites greater than in B-sites and this becomes a decisive factor in determining the final composition.

Electrical Characterization: The conductivity relationship with temperature is shown in Figure 4 for the $Mn_xCo_{1-x}Al_2O_4$ compounds with $0.05 \leq x \leq 0.95$. The results of DC electrical measures analysis presents a typical plot of temperature dependence resistivity for a range of measuring temperatures from 523 K to 823 K continuously. This linear decrease in resistivity as the temperature increases is a feature of semiconductor behavior. The transport mechanism is governed by the increased hopping rate attributed to the enhancement in thermally activated drift mobility of charge carriers. At low temperatures, the samples presented $10^{10}\Omega$.cm values for resistivity and indicate that is very resistive for semiconductor oxides(Philip and Kutty, 1999).On the other hand, in higher temperatures, these values reached the order of $10^6\Omega$.cm (Fig. 4). Activation energies were calculated by the Arrhenius equation and the values obtained were close to 0.30 eV on average. According to some studies(Molenda *et al*., 2003; Radhapiyari *et al*., 2000; Taguchi *et al*., 2009), the conduction mechanism depending on the activation energy of the system. Thisenergy can be either predominantly associated with ionic conduction for high energy values or attributed to electron hopping for low values of activation energy. Therefore, as reported by Radhapiyari*etal*.(Radhapiyari *et al*., 2000), since values found in this study are within the activation energy range between 0.22 eV and 0.75 eV, the electrons hopping have a probable predominance as charge carriers responsible for the electrical conduction of the $Mn_xCo_{1-x}Al_2O_4$ system. As previously mentioned, the increase in manganese ions promoted a redistribution by the occupation of B-sites, that favoring exchanges between Mn^{2+} and Mn^{3+} ions and contributing to the conduction process. In contrast, cobalt ions in B-sites tend to inhibit electron hopping between manganese ions, increasing the material resistivity.

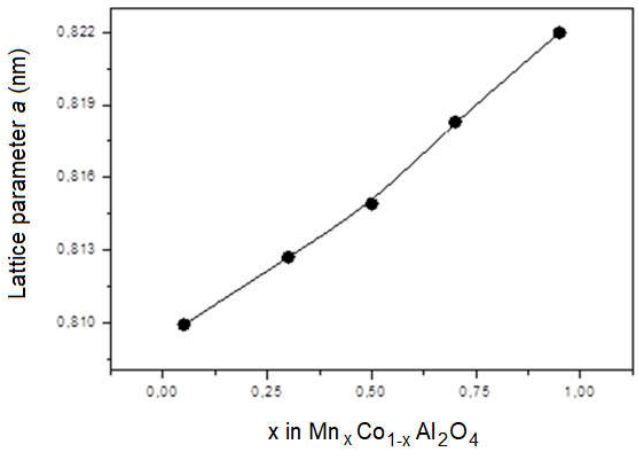

Figure 3. Lattice parameter variation by manganese content according to x molar fraction of the $Mn_xCo_{1-x}Al_2O_4$, with $0.05 \leq x \leq 0.95$

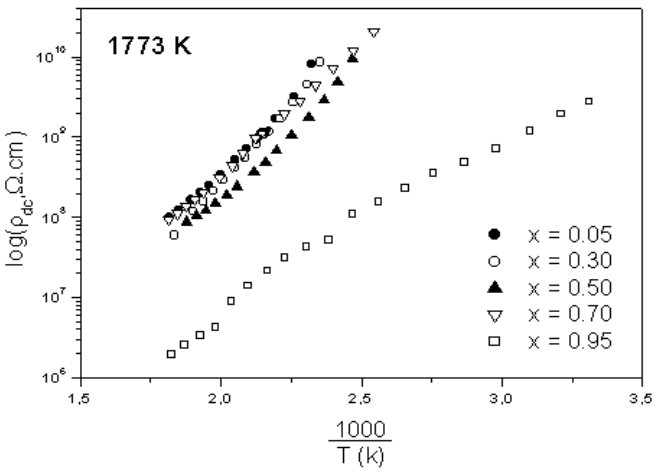

Figure 4. Arrhenius plot of $Mn_xCo_{1-x}Al_2O_4$ samples with $0.05 \leq x \leq 0.95$

In electrical DC measurements, lower resistance values were observed at higher temperatures. In this way, ac electrical measurements were taken by impedance spectroscopy at 623 K in the frequency range of 5 Hz-13 MHz. The electrical response of samples was analyzed through equivalent circuits applying an AC electric field. Their impedance diagrams or Nyquist plots, imaginary part Z" against the real part Z', are shown in Figure 5. The impedance spectroscopy technique was employed to obtain information about charge transport features in the material. To examine and distinguish between the contribution of the grain and the grain boundaries in the conduction mechanisms.Nyquist plots indicated the presence of two semicircles, a small one at a higher frequency region, and a large one at a lower frequency region.

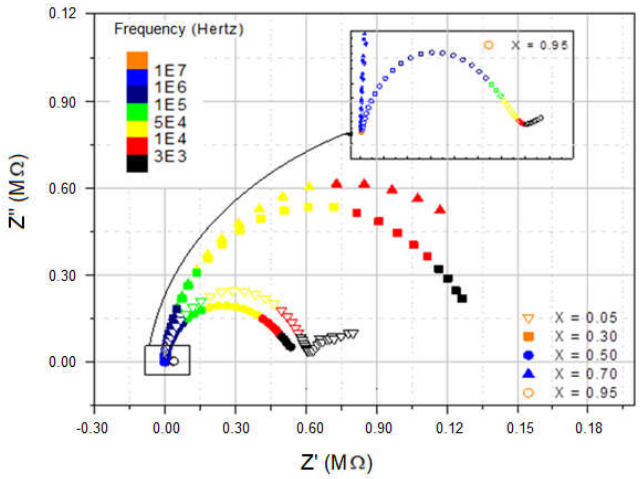

Figure 5. Impedance spectroscopy of $Mn_xCo_{1-x}Al_2O_4$ samples realized at 623 K with $0.05 \leq x \leq 0.95$

These semicircles depict the charge transfer resistance in the material and they also correspond to the existence of two different relaxation processes attributed to the grain (high frequency) and grain boundaries (low frequency).(Ngai and León, 1999)The grain growth occurs due to the sintering process and its size is directly related to the semicircle. This relationship can be noticed in Nyquist plots, where the larger grain size implies greater resistance and, therefore, a greater semicircle.(De Florio and Muccillo, 1999; Fan and Sale, 2000; Ponpandian *et al.*, 2002) The measure of resistance is obtained by fitting equivalent series circuits to take the intercept of the curve on the real part of the Nyquist plot(Barsoukov and Macdonald, 2005). Among the compositions studied here, the one with the lowest resistance was the$Mn_{0.95}Co_{0.05}Al_2O_4$ compound, because showed the smallest semicircle corroborating with the result obtained in DC electrical measurements. That can be seen in the enlarged portion of the curve at the high-frequency region in Figure 5. The contributions of grain R_g and grain boundaries R_{gb} resistivity are determined as a function of real part Z' according to the variation of frequency ϖ.(Wang et al., 1999) To $\varpi \rightarrow 0$, the values obtained of resistivity were due to the contributions of grain and grain boundaries ($Z' = R_g + R_{gb}$), and to $\varpi \rightarrow \infty$, there was only the contribution of the grain ($Z' = R_g$) and the samples exhibited lower values of resistivity.

Table 1. Results of impedance analysis of the $Mn_xCo_{1-x}Al_2O_3$ samples

x Fraction	R_g (Ω) ($\varpi \rightarrow \infty$)	$R_g + R_{gb} \approx R_{gb}$ (Ω) ($\varpi \rightarrow 0$)	$\approx \sigma_{gb}(\mu\Omega^{-1})$
0.05	64	6.1E5	1.6
0.30	42	12.2E5	0.82
0.50	68	52.2E5	0.19
0.70	47	14.3E5	0.69
0.95	275	0.34E5	30.3

Table 1 shows the estimated resistivity values of the samples. These values were obtained by intercepts of semicircles, according to the complex impedance spectra. In low frequency, there was a tendency to increase the resistance values with the increase in Mn content up to x = 0.50 and to $x \geq 0.70$ the resistance values decreased. Probably, the Mn incorporation has led to the slow charge transfer process within the material and enlarged resistance values up to x = 0.50, and the opposite was verified to $x \geq 0.70$. In high frequency, it was not observed the same that to low frequency, the resistance values oscillated as the Mn content increased. In all cases, the materials showed very low resistance, perhaps attributed to contributions from discontinuity in the charge transfer process at the solid oxide/electrode interface or intrinsic resistance of the oxides. Among the studied compositions, the higher conductivity σ of $Mn_xCo_{1-x}Al_2O_4$ system was obtained for the greatest Mn content. Despite the grain having a higher resistance value compared to the other compositions, the contribution of grain boundaries remained prevalent, although it has been minimized. This may be attributed to increased mobility of the charge carriers in the lattice associated with the ambivalent behavior of aluminum as donor and acceptor. The alumina shifts the upturn region to higher current density due to an increase in the conductivity of the $Mn_{0.50}Co_{0.50}Al_2O_4$ grains(Houabes et al., 2005).

CONCLUSION

XRD analysis indicated the presence of Al_2O_3 and $Mn_xCo_{1-x}Al_2O_4$ phases in the samples. The Rietveld method used to analyze the spinel phase showed that the addition of Mn^{2+} ions promoted the increase of the lattice parameters. The high preference of Mn^{2+} for tetrahedral sites induced the migration of Co^{2+} ions to octahedral sites. The electrical measurements of the $Mn_xCo_{1-x}Al_2O_4$ system indicated a characteristic semiconductor behavior. The highest conductivity value obtained relates to the highest amount of Mn observed in botch DC and AC electrical measurements. Samples with a substantial amount of Co^{2+} ions act as inhibitors of exchange among Mn^{2+} and Mn^{3+} ions in octahedral sites. These samples presented higher values of resistivity. Besides, the obtained activation energy values indicated the electron hopping as the same conduction mechanism for all compounds.

Acknowledgment: Federal University of São Carlos – UFSCar.

REFERENCES

Abaide, E.R., Anchieta, C.G., Foletto, V.S., Reinehr, B., Nunes, L.F., Kuhn, R.C., Mazutti, M.A., Foletto, E.L., 2015. Production of copper and cobalt aluminate spinels and their application as supports for inulinase immobilization. Mater. Res. 18, 1062–1069. https://doi.org/10.1590/1516-1439.031415

Barsoukov, E., Macdonald, J.R., 2005. Impedance Spectroscopy: Theory, Experiment, and Applications, Impedance Spectroscopy: Theory, Experiment, and Applications. https://doi.org/10.1002/0471716243

Barth, T.F.W., Posnjak, E., 2014. Spinel structures: with and without variate atom equipoints. Zeitschrift für Krist. - Cryst. Mater. 82. https://doi.org/10.1524/zkri.1932.82.1.325

Barth, T.F.W., Posnjak, E., 1931. The spinel structure: An example of variate atom equipoints. J. Washingt. Acad. Sci. https://doi.org/10.2307/24529279

Bleicher, L., Sasaki, J.M., Paiva Santos, C.O., IUCr, 2000. Development of a graphical interface for the Rietveld refinement program DBWS. J. Appl. Crystallogr. 33, 1189–1189. https://doi.org/10.1107/S0021889800005410

Bolt, P.H., Habraken, F.H.P.M., Geus, J.W., 1998. Formation of nickel, cobalt, copper, and iron aluminates from α- and γ-alumina-supported oxides: A comparative study. J. Solid State Chem. 135. https://doi.org/10.1006/jssc.1997.7590

De Florio, D.Z., Muccillo, R., 1999. Sintering of zirconia-yttria ceramics studied by impedance spectroscopy. Solid State Ionics 123. https://doi.org/10.1016/S0167-2738(99)00093-4

El Habra, N., Crociani, L., Sada, C., Zanella, P., Casarin, M., Rossetto, G., Carta, G., Paolucci, G., 2007. MOCVD of CoAl2O4 thin films from {CO[AI(O iC3HT)4]2} as precursor. Chem. Mater. 19, 3381–3386. https://doi.org/10.1021/cm0615931

Fan, J., Sale, F.R., 2000. The microstructures, magnetic properties and impedance analysis of Mn-Zn ferrites doped with B2O3. J. Eur. Ceram. Soc. 20. https://doi.org/10.1016/s0955-2219(00)00230-2

Gallaghe, P.K., Obryan, H.M., Schrey, F., Monforte, F.R., 1969. Preparation of a nickel ferrite from coprecipitated Ni0.2Fe0.8C2O4.2H2O. Am. Ceram. Soc. Bull. 48, 1053–1059.

Gomes, K.Q., 2003. Caracterização estrutural e elétrica de óxidos semicondutores do tipo espinélio. UFSCar, São Carlos.

Hotovy, I., Huran, J., Spiess, L., Hascik, S., Rehacek, V., 1999. Preparation of nickel oxide thin films for gas sensors applications. Sensors Actuators, B Chem. 57, 147–152. https://doi.org/10.1016/S0925-4005(99)00077-5

Houabes, M., Bernik, S., Talhi, C., Bui, A., 2005. The effect of aluminium oxide on the residual voltage of ZnO varistors. Ceram. Int. https://doi.org/10.1016/j.ceramint.2004.09.004

Jacob, K.T., Fitzner, K., 1977. Ion-exchange equilibria between (Mn, Co)O solid solution and (Mn, Co) Cr2O4 and (Mn, Co) Al2O4 spinel solid solutions at 1100° C. J. Mater. Sci. 12. https://doi.org/10.1007/BF00540270

Jacob, K.T., Raj, S., Rannesh, L., 2007. Vegard's law: A fundamental relation or an approximation? Int. J. Mater. Res. 98, 776–779. https://doi.org/10.3139/146.101545

Lambregts, M.J., Frank, S., 2004. Application of Vegard's law to mixed cation sodalites: A simple method for determining the stoichiometry. Talanta 62, 627–630. https://doi.org/10.1016/j.talanta.2003.09.007

Microsoft, 2000. VEE Pro user's guide. Agil. Technol. Inc.

Molenda, J., Swieerczek, K., Marzee, J., Liu, R.S., 2003. Charge transport mechanism in LiCoyMn2-yO4 cathode material. Solid State Ionics 157, 101–108.

Ngai, K.L., León, C., 1999. Recent advances in relating macroscopic electrical relaxation data to microscopic movements of the ions in ionically conducting materials. Solid State Ionics 125, 81–90. https://doi.org/10.1016/S0167-2738(99)00161-7

Oh, S.W., Myung, S.T., Kang, H.B., Sun, Y.K., 2009. Effects of Co doping on Li[Ni0.5CoxMn1.5-x]O4 spinel materials for 5 V lithium secondary batteries via Co-precipitation. J. Power Sources 189, 752–756. https://doi.org/10.1016/j.jpowsour.2008.08.022

Philip, J., Kutty, T.R.N., 1999. Colossal magnetoresistance of oxide spinels, CoxMn3-xO4. Mater. Lett. 39. https://doi.org/10.1016/S0167-577X(99)00026-9

Ponpandian, N., Balaya, P., Narayanasamy, A., 2002. Electrical conductivity and dielectric behaviour of nanocrystalline NiFe2O4 spinel. J. Phys. Condens. Matter 14. https://doi.org/10.1088/0953-8984/14/12/311

Porta, P., Anichini, A., Bucciarelli, U., 1979. Distribution of nickel ions among octahedral and tetrahedral sites in NixZn1-xAl2O4 spinel solid solutions. J. Chem. Soc. Faraday Trans. 1 Phys. Chem. Condens. Phases 75, 1876–1887. https://doi.org/10.1039/F19797501876

Posnjak, E., Barth, T.F.W., 1931. A new type of crystal fine-structure: Lithium ferrite (Li2O·Fe2O3). Phys. Rev. 38. https://doi.org/10.1103/PhysRev.38.2234

Pradhan, S.K., Dalal, B., Sarkar, A., De, S.K., 2019. Spectroscopic and magnetic investigations of a spin-frustrated Mn-doped CoAl2O4 spinel. Phys. Chem. Chem. Phys. 21, 842–850. https://doi.org/10.1039/c8cp07140c

Radhapiyari, L., Phanjoubam, S., Sarma, H.N.K., Prakash, C., 2000. Influence of Co2+ on the electrical and magnetic properties of Li-Sb ferrites. Mater. Lett. 44, 65–69. https://doi.org/10.1016/S0167-577X(00)00003-3

Rietveld, H.M., 1969. A profile refinement method for nuclear and magnetic structures. J. Appl. Crystallogr. 2, 65–71. https://doi.org/10.1107/S0021889869006558

Schwake, A., Geuking, H., Cammann, K., 1998. Application of a New Graphical Fitting Approach for Data Analysis in Electrochemical Impedance Spectroscopy. Electroanalysis 10, 1026–1029. https://doi.org/10.1002/(SICI)1521-4109(199810)10:15<1026::AID-ELAN1026>3.0.CO;2-H

Shannon, R.D., 1976. Revised effective ionic radii and systematic studies of interatomic distances in halides and chalcogenides. Acta Crystallogr. Sect. A 32, 751–767. https://doi.org/10.1107/S0567739476001551

Sickafus, K.E., Wills, J.M., Grimes, N.W., 2004. Structure of Spinel. J. Am. Ceram. Soc. 82, 3279–3292. https://doi.org/10.1111/j.1151-2916.1999.tb02241.x

Taguchi, H., Hirata, K., Kido, H., Takeda, Y., Kato, M., Hirota, K., 2009. Hopping conductivity of distorted K2NiF4-type (Ca1+xNd1-x)CrO4. Solid State Sci. 11. https://doi.org/10.1016/j.solidstatesciences.2009.03.011

Verwey, E.J.W., Heilmann, E.L., 1947. Physical properties and cation arrangement of oxides with spinel structures I. Cation arrangement in spinels. J. Chem. Phys. 15, 174–180. https://doi.org/10.1063/1.1746464

Wang, D.J., Qiu, J., Guo, Y.C., Gui, Z.L., Li, L.T., 1999. Grain boundary effects in NTC-PTC composite thermistor materials. J. Mater. Res. 14. https://doi.org/10.1557/JMR.1999.0019

Youl Bae, H., Man Choi, G., 1999. Electrical and reducing gas sensing properties of ZnO and ZnO-CuO thin films fabricated by spin coating method. Sensors Actuators, B Chem. 55, 47–54. https://doi.org/10.1016/S0925-4005(99)00038-6

Young, R.A., Sakthivel, A., Moss, T.S., Paiva-Santos, C.O., 1995. Rietveld analysis of X-ray and neutron powder diffraction patterns. User's guide to program DBWS-9411.

Zasada, F., Gryboś, J., Indyka, P., Piskorz, W., Kaczmarczyk, J., Sojka, Z., 2014. Surface structure and morphology of M[CoM′]O4 (M = Mg, Zn, Fe, Co and M′ = Ni, Al, Mn, Co) spinel nanocrystals-DFT+U and TEM screening investigations. J. Phys. Chem. C 118, 19085–19097. https://doi.org/10.1021/jp503737p

****